

New York City Impacts on a Regional Heat Wave

LUIS E. ORTIZ AND JORGE E. GONZALEZ

Department of Mechanical Engineering, The City College of New York, New York, New York

WEI WU^a AND MARTIN SCHOONEN

Environmental and Climate Sciences Department, Brookhaven National Laboratory, Upton, New York

JEFFREY TONGUE

National Weather Service New York Office, Upton, New York

ROBERT BORNSTEIN

Department of Meteorology and Climate Science, San Jose State University, San Jose, California

(Manuscript received 6 May 2017, in final form 16 January 2018)

ABSTRACT


Heat waves are projected to increase in magnitude and frequency throughout this century because of increasing global temperatures, making it critically important to acquire improved understanding of their genesis and interactions with large cities. This study presents an application of the method of factor separation to assess combined impacts of a synoptic-scale heat wave, urban land cover, and urban energy and momentum fluxes on temperatures and winds over New York City, New York, via use of high-resolution simulations (1-km grid spacing) with an urbanized version of the Weather Research and Forecasting (WRF) Model. Results showed that factors behaved different throughout the day, with synoptic conditions dominating afternoon temperature contributions ($>7^{\circ}\text{C}$). At night, combined urban surface factors contributed over 5°C during the heat wave and up to 1.5°C on non-heat-wave days. Positive interactions among all factors during morning and nighttime indicate an amplification of the urban heat island of up to 4°C during the heat wave. Midtown Manhattan vertical cross sections, where urban canopies are most dense, showed a change in the sign (from positive to negative) of the contribution of the urban fluxes between night and day below 500 m, possibly as a result of decreased radiative cooling from trapping by buildings and increased thermal storage by buildings as well as frictional effects that oppose the incoming warm air.

1. Introduction

Extreme-heat events are one of the most damaging weather phenomena, impacting human health, infrastructure, and the natural environment. Heat waves, typically defined as a series of days with higher than

climatological maximum temperatures (Robinson 2001), were the leading cause of weather-related fatalities in the United States between 2005 and 2014, as reported by National Weather Service (2015). High temperatures also stress the electric grid because of increased demand for space cooling (Le Comte and Warren 1981; Santamouris et al. 2001; Miller et al. 2008), leading to increased operational costs.

As temperature increases, so do mortality and hospitalizations in vulnerable groups such as the young and the elderly (McGeehin and Mirabelli 2001; Basu 2009), a problem that urban heat islands (UHI) exacerbate in cities (Curriero et al. 2002; Anderson and Bell 2010; Madrigano et al. 2015). With heat waves projected to increase in magnitude, duration, and frequency because of global warming (Meehl and Tebaldi 2004), it

 Denotes content that is immediately available upon publication as open access.

^a Current affiliation: Coast Survey Development Laboratory, Office of Coast Survey, NOAA/National Ocean Service, Silver Spring, Maryland.

Corresponding author: Luis E. Ortiz, lortiz10@citymail.cuny.edu

is important to understand interactions between urban environments and their surroundings during these potentially catastrophic events.

New York City (NYC), New York, is divided into five boroughs covering almost 800 km², with a greater metropolitan area of over 17 000 km². This heavily urbanized region has been the focus of several efforts to characterize its UHI and its adverse impacts. The NYC UHI is strongest during nighttime, with a summer average of 4°C and maximum values occurring when surface wind speeds are less than 2.6 m s⁻¹ (Gedzelman et al. 2003). Sea breezes play an important role in UHI development, with daytime easterly flows cooling coastal and inner-city areas. Easterly or southeasterly breezes delayed UHI development but did not reduce its magnitude much. Bornstein and Thompson (1981) showed that NYC retarded slow-moving fronts and sea breezes, increasing pollutant concentrations over the city.

Bornstein (1968) described the vertical structure of the NYC UHI on the basis of morning airborne observations, finding that UHIs extended from the surface to 300–500 m, with elevated weak inversion layers near the UHI top. Gaffin et al. (2008) showed that, because of the complex nature of its urban morphology and its interactions with seasonal wind patterns, the NYC UHI exhibits both spatial and temporal variations of as much as 2°C between inner-city sites. These spatial differences are (in part) due to the heterogeneity of the urban environment, with building and street geometry affecting the UHI intensity (Oke 1988).

With the availability of increasingly powerful computing resources, high-resolution simulations of urban climate have focused on characterization of the spatial and temporal variabilities of UHIs in a variety of cities, as well as on mitigation strategies to reduce their negative impacts. For example, Meir et al. (2013) used the Coupled Ocean–Atmosphere Mesoscale Prediction System mesometeorological model with a high-resolution (1-km grid spacing) multilayer urban canopy parameterization to forecast NYC UHI, finding that simulated high-resolution temperatures and sea breezes were more accurate than from the operational North American Mesoscale Forecast System (NAM), especially near the coast. Ronda et al. (2017) more recently showed improved near-surface weather-forecast performance at subkilometer resolutions (100 m) using a modified version of the Weather Research and Forecasting (WRF) Model with a single-layer urban canopy model. They found reduction in mean absolute error across all forecast lead times, resolving sub-neighborhood-scale processes such as effects from nearby water bodies and heterogeneous urban cover.

Other studies have focused on use of urbanized weather models to assess UHI contributions from different urban parameters; for example, Ryu and Baik (2012) used idealized simulations with the WRF Model

with a single-layer urban canopy model to separate the impacts of urban surfaces, 3D urban morphology (i.e., building canyons), and urban anthropogenic heat on UHI development. They found that contributions from urban morphology to UHI magnitude were negative during daytime and positive at night. Li and Bou-Zeid (2013) used analytical, numerical, and observational analyses to study interactions between UHIs and heat waves in Baltimore, Maryland. They found that heat waves increase simulated urban 2-m air temperatures by nearly 2°C at night and 0.5°C during daytime as a result of decreased urban wind speeds and a lack of evaporative cooling over impervious surfaces.

Whereas previous studies of UHI development during heat waves used either idealized numerical models and analytical formulations (Li and Bou-Zeid 2013; Ryu and Baik 2012) or very-high-resolution limited-area models (Ronda et al. 2017) to quantify impacts from buildings on atmospheric dynamics, this study is the first to assess relative contributions to NYC urban temperatures and winds from a synoptic heat wave, urban fluxes, and impervious surfaces by use of a high-resolution urbanized mesoscale model via application of the method of factor separation.

2. Data and methods

a. Heat-wave case study

On 4–8 July 2010, a high pressure system (Fig. 1) stagnated over the U.S. East Coast, inducing a southwesterly regional warm airflow over the NYC region. This system persisted until 9 July 2010, when it moved farther away from the coast, allowing for cooler conditions. The NYC National Weather Service regional office declares a heat wave with three or more consecutive days with maximum 2-m temperatures (hereinafter referred to as temperatures) over 32.2°C (90°F). This particular event was significant as several stations throughout the NYC region recorded temperatures of at least 39°C. Although this event falls in the 96th percentile in terms of maximum temperature and 64th percentile of all event durations between 1973 and 2016, synoptic conditions are fairly typical of heat-wave formation, with a persistent “blocking high” occurring over or near the affected area (Charney and DeVore 1979).

b. Model configuration

Simulations in this study used the WRF Model (Skamarock et al. 2008), version 3.5.1, a state-of-the-art numerical weather prediction system that was developed and is maintained by the National Center for Atmospheric Research. Three simulation cases with

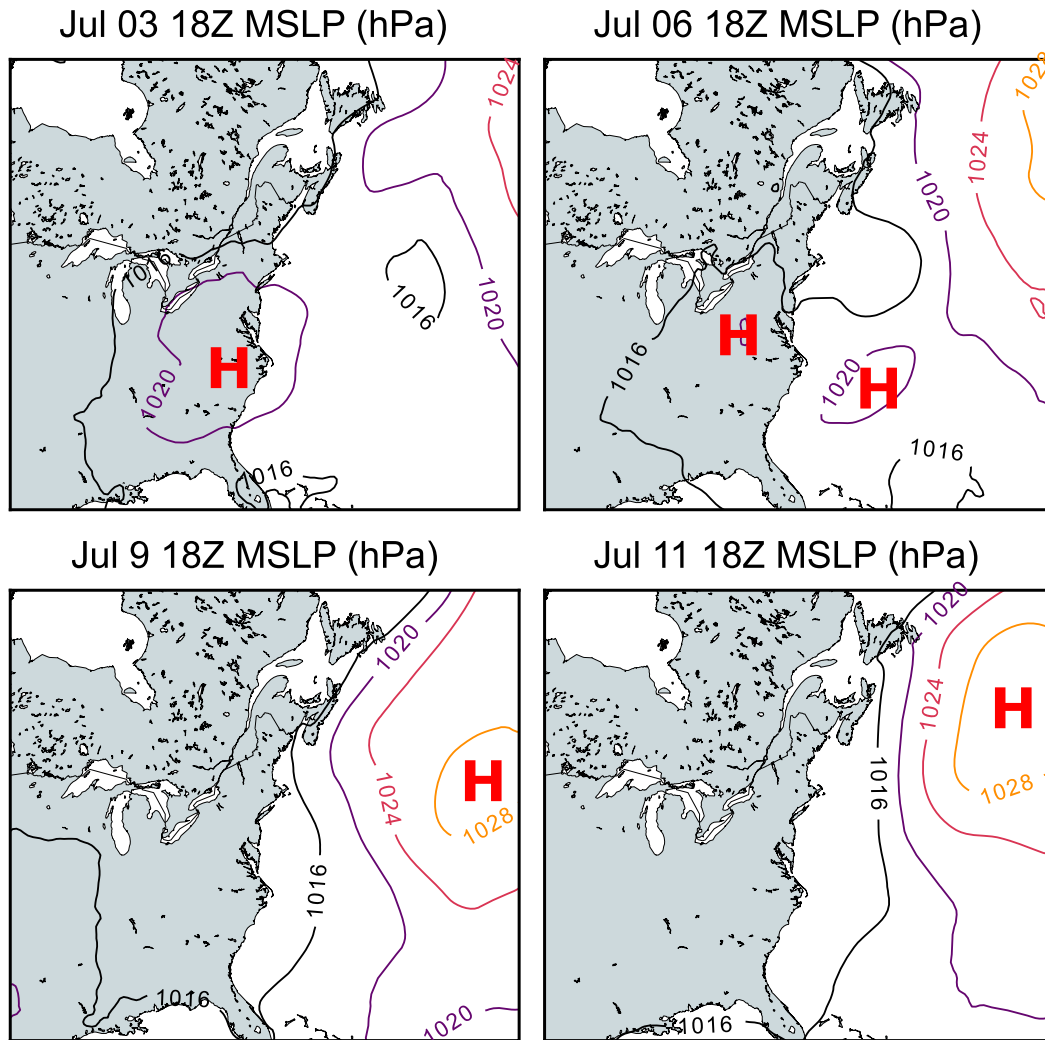


FIG. 1. NARR mean sea level pressure (labeled MSLP) contours (hPa) at 1800 UTC 3, 6, 9, and 11 Jul showing progression of the persistent high pressure system leading to heat-wave conditions across the eastern United States.

varying land cover and urban parameterizations were developed to study the above heat wave.

Model physics for all simulations followed the work of Gutiérrez et al. (2015b). The microphysics scheme used was the WRF single-moment six-class microphysics scheme (WSM6) of Hong and Lim (2006). For longwave radiation, the Rapid Radiative Transfer Model of Mlawer et al. (1997), which considers impacts from water vapor, carbon dioxide, and methane, among others, was used. Also used were the shortwave parameterization of Dudhia (1989); the Kain–Fritsch cumulus scheme (active only on the coarse d02 and d03 domains) (Kain 2004), which accounts for moist downdrafts and updrafts as well as entrainment and detrainment; the “Noah” land surface model (Tewari et al. 2004), which integrates four layers of soil moisture and temperature at nonurban grid

points; and the “BouLac” PBL scheme (Bougeault and Lacarrere 1989), which uses TKE prediction and was designed for use in urban parameterizations. The urban multilayer scheme is composed of the building environment parameterization (BEP) and building energy model (BEM) of Martilli et al. (2002) and Salamanca et al. (2010), respectively, both of which consider anthropogenic heat exchanges.

The simulation region (Fig. 2) consists of an outer domain (d01) and two nested grids (d02, d03) with horizontal resolutions of 9, 3, and 1 km, respectively. The two nested domains use two-way nesting in which calculations from the finer-resolution grid are used to update coarser-resolution grid points. All domains use 50 vertical levels, with 15 within the bottom 3 km. Observational nudging was not used. The model is initialized with North

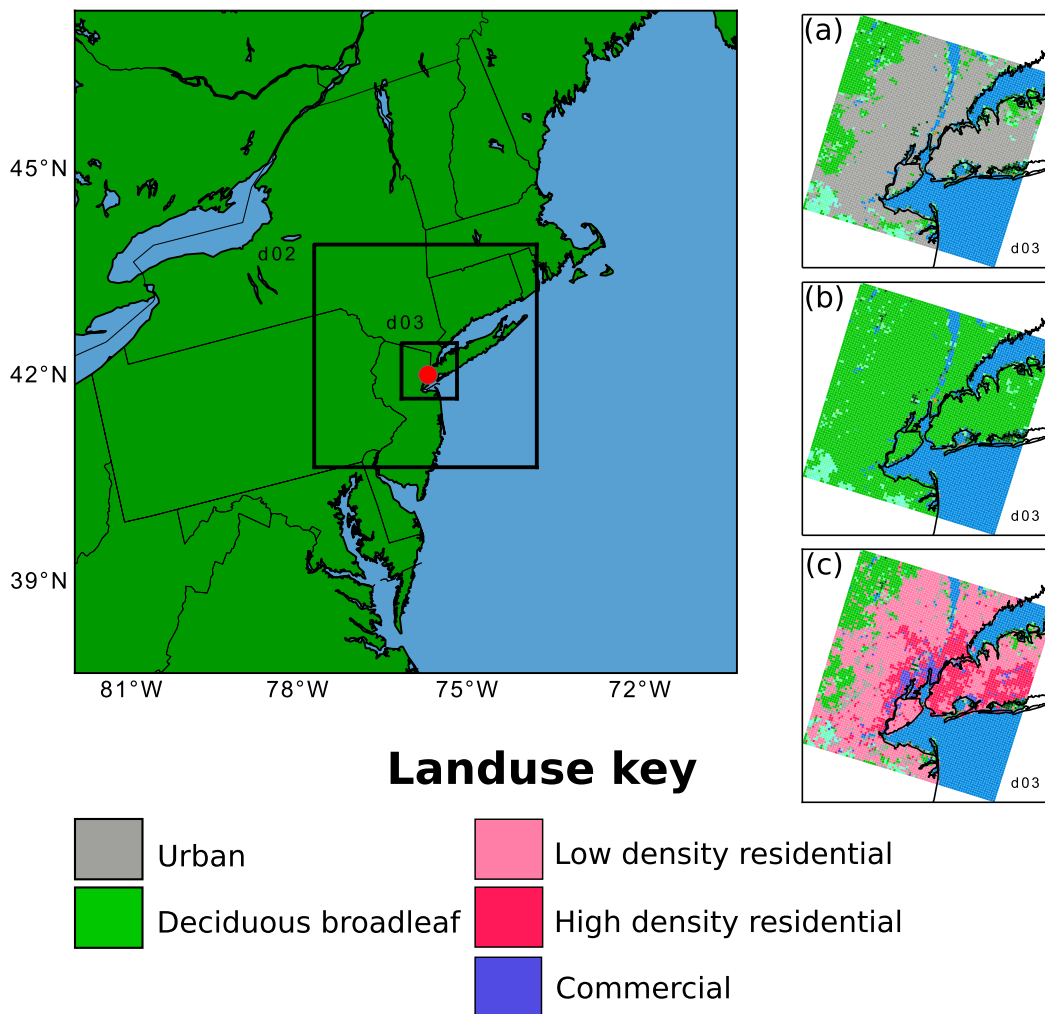


FIG. 2. WRF domains, with coarse domain (d01: entire plot) and inner domains d02 and d03 (black-outlined boxes); the red dot marks NYC. Also given is the urban land use for each WRF simulation: (a) MODIS 20-category (single urban) for the control simulation, (b) no urban (urban grids over the NYMA are changed to deciduous broadleaf) for the forest simulation, and (c) disaggregation of urban into three classes for the urban simulation.

American Regional Reanalysis (NARR; Mesinger et al. 2006) 32-km-resolution data starting on 3 July 2010 and ending on 11 July 2010, with a spinup period of 12 h.

c. Simulation setup

The study uses three simulations partitioned into six cases to study the sensitivity of local NYC weather to combination effects from the heat wave and changes in urban land cover and urban fluxes. The control simulation

(Table 1) uses standard WRF, with the Noah land surface model and the MODIS 20-class land-use categories but with no urban parameterization (Fig. 2a). In the forest simulation, all MODIS class-13 (urban and built up) grid points over the New York metropolitan area (NYMA) are changed to deciduous broadleaf forests (Fig. 2), which is the most common nonurban land use in the Northeast. To better approximate nonurban conditions, all soil moisture levels over the modified grid points were increased to

TABLE 1. Simulations and corresponding treatments of land cover and urban surfaces.

Simulation	Land cover	Urban parameterization
Control	20-class MODIS	One urban class
Forest	Modified 20-class MODIS	None
Urban	PLUTO	Three urban classes BEP-BEM + urban hydrology + cooling tower

TABLE 2. Mapping of PLUTO land-use categories to National Land Cover Database three-category urban classification.

WRF urban categories	PLUTO land-use classification
Low-density residential	One- and two-family buildings Parking facilities
High-density residential	Multifamily walk-up buildings Multifamily elevator buildings
Commercial	Industrial and manufacturing Mixed residential and commercial Commercial and office Transportation and utility Public facilities and institutions

match the profile of the closest deciduous broadleaf forest points across all model domains.

In the urban simulation, MODIS class-13 grid points are disaggregated into three new classes: low-density residential, high-density residential, and commercial (Fig. 2c). These urban categories are derived from the New York Primary Land Use Tax Lot Output (PLUTO) land-use data, mapping the specific categories as detailed in Table 2. Several urban parameters (i.e., building-area fraction, ratio of building surface area to height, and height) are computed from PLUTO on a building-lot basis and aggregated at the 1-km resolution of domain d03 as detailed by Gutiérrez et al. (2015c), with the rest taken from the National Urban Database and Access Portal Tool (NUDAPT) 1-km dataset (Burian et al. 2008). BEP and BEM urban physics are also modified to include a variable drag coefficient C_{deq} as a function of building-plan-area fraction λ_p (Gutiérrez et al. 2015c) as follows:

$$C_{\text{deq}}(\lambda_p) = \begin{cases} 3.32\lambda_p^{0.47} & \text{for } \lambda_p \leq 0.29 \\ 1.85 & \text{for } \lambda_p > 0.29 \end{cases}$$

The cooling tower parameterization of Gutiérrez et al. (2015a) quantifies latent heat fluxes from air-conditioning evaporative-cooling systems, which reduces the overpredicted temperature values observed in simulations with previous BEP–BEM formulations. The urban hydrological parameterization of Gutiérrez (2016) is likewise used, because it estimates urban canyon moisture and latent heat fluxes from accumulated water in impervious and vegetated surfaces from the accumulated water in urban impervious (e.g., pavements and roofs) surfaces, better accounting for water retention and runoff. Its latent heat fluxes from urban vegetation account for evapotranspiration from low vegetation (e.g., grass) and also account for vertical soil diffusion.

Model performance is evaluated with surface measurements from a ground-station network and a radar wind profiler (RWP). All measurements are from the NYCMetNet archive (Arend et al. 2009), which includes over 500 NYMA stations. Data from stations with less than 75% temporal coverage were discarded, leaving 344 stations over the NYMA. The RWP is located at the Liberty Science Center in Jersey City, New Jersey, west of the southern tip of Manhattan Island (Fig. 3). The root-mean-square error (RMSE) is used as a performance metric; that is,

$$\text{RMSE} = \left[\frac{\sum_{t=1}^n (\hat{y}_t - y_t)^2}{n} \right]^{1/2},$$

where \hat{y}_t and y_t are model and observations values, respectively, at time t and n is the number of samples. Model performance is assessed for a simulation with and without modified urban physics in BEP–BEM.

d. Factor-separation analysis

This study employs the method of factor separation (Stein and Alpert 1993) to assess urbanization impacts on simulated temperature and wind fields. This approach determines contributions from several factors to any given field and has been applied to study impacts of urban land cover on boundary layer heights and winds (Martilli 2002), as well as effects from urban and vegetation covers in modeling convective systems (Niyogi et al. 2006). Factor separation has also been used to

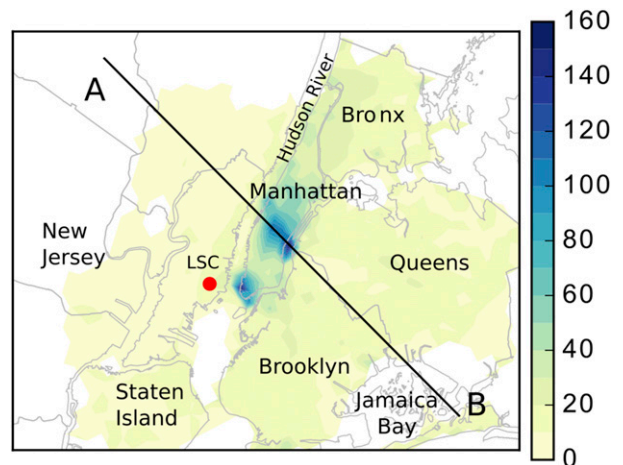


FIG. 3. Building heights (m) at 1-km resolution, where A–B is the plane used in the vertical section analyses. The red dot shows the location of Liberty Science Center, where the RWP is located.

TABLE 3. Factor contributions and corresponding simulation cases.

Case	Simulation/date	Description	Factor contribution
f_0	Forest/9–11 Jul	Baseline: No factors	F_0
f_1	Control/9–11 Jul	Only urban surface	$F_1 - F_0$
f_3	Forest/4–8 Jul	Only heat-wave synoptic conditions	$F_3 - F_0$
f_{12}	Urban/9–11 Jul	Interactions between urban surface and urban fluxes	$F_{12} - F_1$
f_{13}	Control/4–8 Jul	Interactions between urban surface and heat-wave synoptic conditions	$F_{13} - F_1 - F_3 + F_0$
f_{123}	Urban/4–8 Jul	Interaction between all three factors	$F_{123} - (F_{12} + F_{13}) + F_1$

study combined effects from land cover and climate change in California (Sequera et al. 2015) and San Juan, Puerto Rico (Comarazamy et al. 2013).

The analysis separates contributions from several physical processes to a predicted field, in this case temperature and winds. Three factors are considered: impervious land cover, urban morphology and processes (referred to as *urban fluxes*), and synoptic heat-wave conditions (factors 1, 2, and 3, respectively). Factor-separation analysis requires that the factors of interest are turned off and on to evaluate their relative impacts. For the urban land surface factor, the *on* state is defined with the use of standard land cover (control simulation) and the *off* state uses the forest simulation. For the urban fluxes factor, the *on* state is defined by the use of the modified BEP–BEM (urban simulation). For the heat-wave factor, two periods are employed, 4–8 July (heat wave) and 9–11 July (no heat wave), as a way to remove the synoptic effects from the high pressure system.

The number of simulations needed to account for the contributions of n factors and their interactions is normally 2^n . For three factors, the relative contribution of a field and their interactions f is given by

$$\begin{aligned}
 f_0 &= F_0, \\
 f_1 &= F_1 - F_0, \\
 f_2 &= F_2 - F_0, \\
 f_3 &= F_3 - F_0, \\
 f_{12} &= F_{12} - (F_1 + F_2) + F_0, \\
 f_{13} &= F_{13} - (F_1 + F_3) + F_0, \\
 f_{23} &= F_{23} - (F_2 + F_3) + F_0, \quad \text{and} \\
 f_{123} &= F_{123} - (F_{12} + F_{13} + F_{23}) + (F_1 + F_2 + F_3) - F_0,
 \end{aligned}$$

where F_i is a simulated field produced from factors $i = 1, 2, \text{ or } 3$ (and any possible combinations between them). The f_0 term represents the baseline field, that is, the net contribution when all effects of interest are turned off. In this case, urban parameterization factors are only activated in the presence of urban grid points (i.e., when factors 1 and 2 are simultaneously present); thus, $F_2 = F_0$ and $F_{23} = F_3$. This results in elimination of single factor

contributions from not only the urban fluxes (f_2) but also from their interaction with the heat wave (f_{23}). The resulting six simplified contributions from each factor and their interactions are detailed in Table 3. Results are presented for 0600 and 1500 LST (UTC – 4h), representing daily minimum and maximum temperatures, for both 2-m fields and a vertical cross section passing through line AB (Fig. 3).

3. Results and discussion

a. Model evaluation

Figure 4 shows RMSE in hourly temperatures between the NYCMetNet observation network stations and the control and urban simulations for 3–8 July 2010. Results show RMSE values ranging between 0.7° and 3°C. Improvements from using multilayer urban parameterization are largest over Manhattan, where RMSE in the urban simulation average 1.8°C, as compared with 2.6°C in the control simulation. Over grid points classified as high-density residential (Brooklyn, Queens, and the Bronx), RMSE values are very close for both simulations, with mean values of 1.8 and 1.9 for control and urban, respectively. This lack of improvement over these areas could be due to a variety of factors such as overestimation of anthropogenic heat in non-commercial grid points, where air-conditioning systems are less widely adopted, as well as mischaracterization of parameterized drag coefficients based solely on the building-plan-area fraction. Model performance decreases with distance from the city toward the north and northwest. This may be indicative of lower-quality surface boundary data inputs as well as the presence of small changes that are not resolved at 1-km horizontal resolution.

Comparison of 6 July 2010 horizontal (X – Y plane) wind profiles from the urban simulation with RWP (Fig. 5) shows that the model generally reproduced observed patterns and diurnal changes throughout but underestimates observed magnitudes. The model also captures the more abrupt changes during the mid-afternoon (1500–1700 LST), possibly because of sea-breeze and synoptic-pattern convergence. Simulations

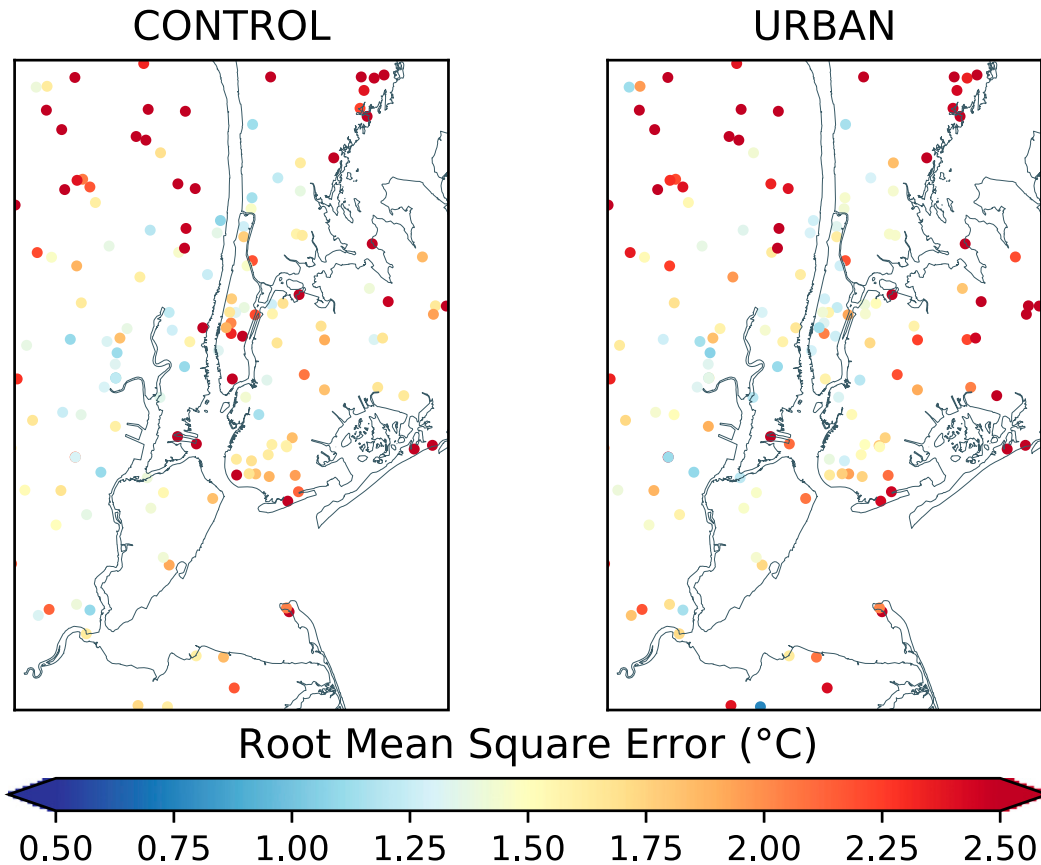


FIG. 4. RMSE of surface air temperatures from the (left) control and (right) urban simulations against NYCMetNet ground stations.

show a slight directional bias as well, missing the vertical wind shear observed in RWP data above 500 m from northwesterly to northeasterly winds.

b. Spatial distributions with all factors

Figures 6a and 6b show the total spatial distribution of temperatures and winds at 0600 and 1500 LST (i.e., with all factors switched on). The plot for daytime hours (Fig. 6b) shows a south-southeast sea breeze, cooling the southern coast of Long Island (including the NYC boroughs of Brooklyn and Queens), which mitigates impacts from urbanization, while displacing the maximum UHI westward, with a magnitude between 2 and 3 K, as described by Gedzelman et al. (2003). The synoptic circulation associated with the heat wave produces west-northwesterly winds that converge with the sea breeze over Manhattan and the northern coast of Brooklyn and Queens. Uptown Manhattan and westward in New Jersey, past the sea-breeze penetration, temperatures reach nearly 39°C.

Along cross section AB (Fig. 6d), a superadiabatic lapse rate is observed near the surface as a result of

intense insolation. This layer is observed over areas with low-rise buildings, where a larger fraction of incoming radiation is more likely to reach the ground surface unimpeded, leading to warmer near-surface air. Above this layer, the air is well mixed. The synoptic flow converges with the sea breeze, generating upward motions. The sea-breeze front is opposed by the synoptic flow, decreasing its overall magnitude, with a return flow starting near 800-m height.

The plot for nighttime hours (Fig. 6a) shows that a weak land breeze from the southwestern and western directions formed, leading to a stronger UHI centered over Brooklyn and Queens, with maximum magnitude between 5 and 6 K. Heavily urbanized areas slow the sea breeze within the urban canopy (below 200 m). Increased surface temperatures over Brooklyn and Queens (38–48 km into the cross section) lead to a weakly stable (nearly neutral) or residual layer, extending to 350-m height. Potential temperatures at this time (Fig. 6c) also show a mixed residual layer over Manhattan (27–37 km into the cross section), which extends to just above maximum building height. West

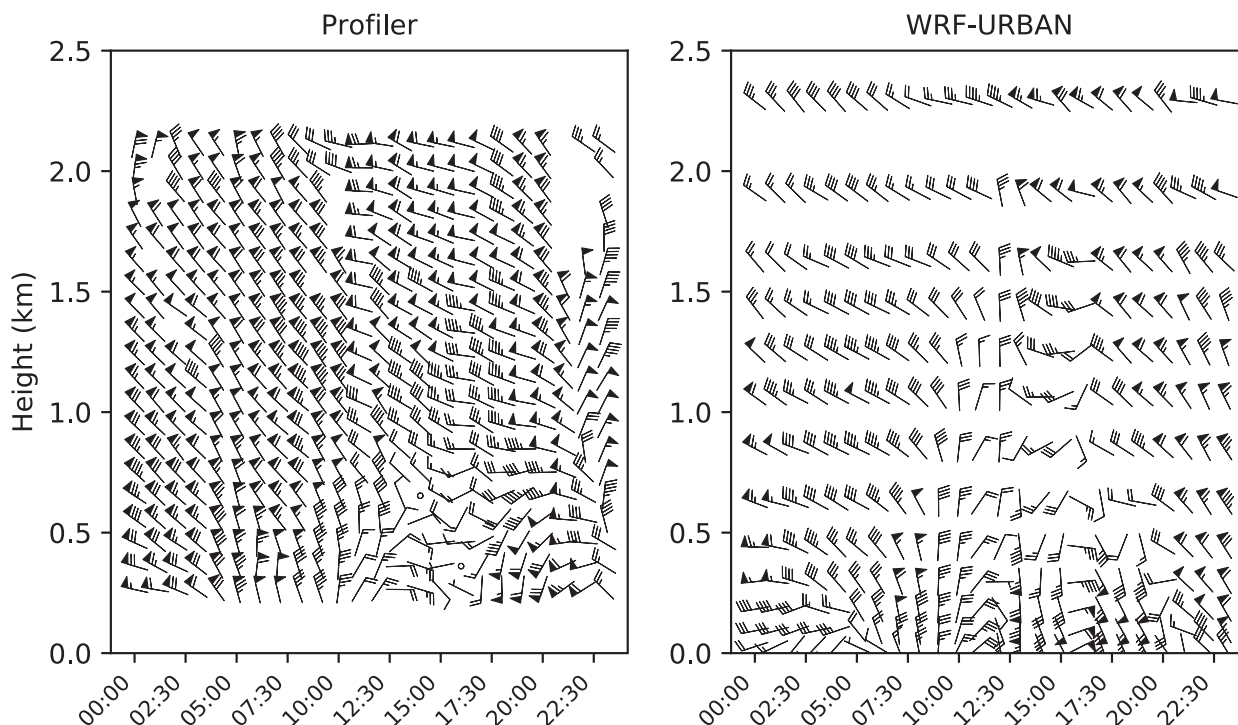


FIG. 5. Horizontal wind profiles (U , V) from (left) the RWP and (right) the urban simulation with all factors turned on. The wind-barb scale is 0.5 , 1.0 , and 5.0 m s^{-1} for half barbs, full barbs, and flags, respectively. Open circles represent winds lower than 0.5 m s^{-1} . Times are LST (UTC - 4h).

of Manhattan, potential temperature profiles show more-stable conditions as added heating associated with the city becomes less prevalent.

c. Factor-separation analysis

1) SURFACE FIELDS

Given the different processes taking place during the early morning and afternoon, factor contributions vary with the diurnal cycle. In the afternoon (1500 LST), contributions to temperature from the urban surface (Fig. 7a) are positive and largest over Brooklyn and Queens and parts of New Jersey across the Hudson River, reaching nearly 2°C . Contributions to the wind field are very small ($0.5\text{--}2 \text{ m s}^{-1}$) and are converging over the city because of additional warming, somewhat enhancing both the anticyclonic and sea-breeze flows. Relative to the total surface field (Fig. 6b), the urban surface is an additive factor to the observed flow patterns.

Meanwhile, interactions between the urban surface and urban fluxes (Fig. 7b) lead to the opposite effect in the flow field, acting against the prevailing sea breeze and southwesterly as shown in Fig. 6a. Tall buildings in downtown and midtown Manhattan increase anthropogenic heat fluxes from air-conditioning use, leading to a weak positive temperature contribution ($0.5^\circ\text{--}1^\circ\text{C}$). This

cooling could be due in part to the radiation blocking from buildings, as well as decreased penetration of the warm anticyclonic air associated with the heat wave. A similar, weaker pattern is observed from the urban surface and heat-wave interaction (Fig. 7c) contribution, which in turn leads to a weaker cooling throughout the NYMA. This factor, however, is negligible (it adds nearly 0°C) over midtown and downtown Manhattan, then turns positive in parts of New Jersey, Brooklyn, and the Bronx.

Synoptic heat-wave conditions (Fig. 7d) dominate temperature contributions throughout the domain, adding over 10°C in most areas. The high pressure system associated with the heat wave generates westerly and northwesterly winds throughout. Southwesterly winds are seen to the south, off the Brooklyn and Queens coastline, possibly because of differential heating between land and the sea surface, contributing somewhat to the sea breeze.

Nonlinear, synergistic interactions among all factors (Fig. 7e) indicate some amplification of the daytime UHI ($0.5^\circ\text{--}2^\circ\text{C}$) over Manhattan, the Bronx, and west of the Hudson River. The coupled nature of air-conditioning systems (as parameterized in BEM) with atmospheric temperature in the urban canopy leads to increased anthropogenic heating in areas with high-rise buildings, in turn resulting in higher temperature contributions

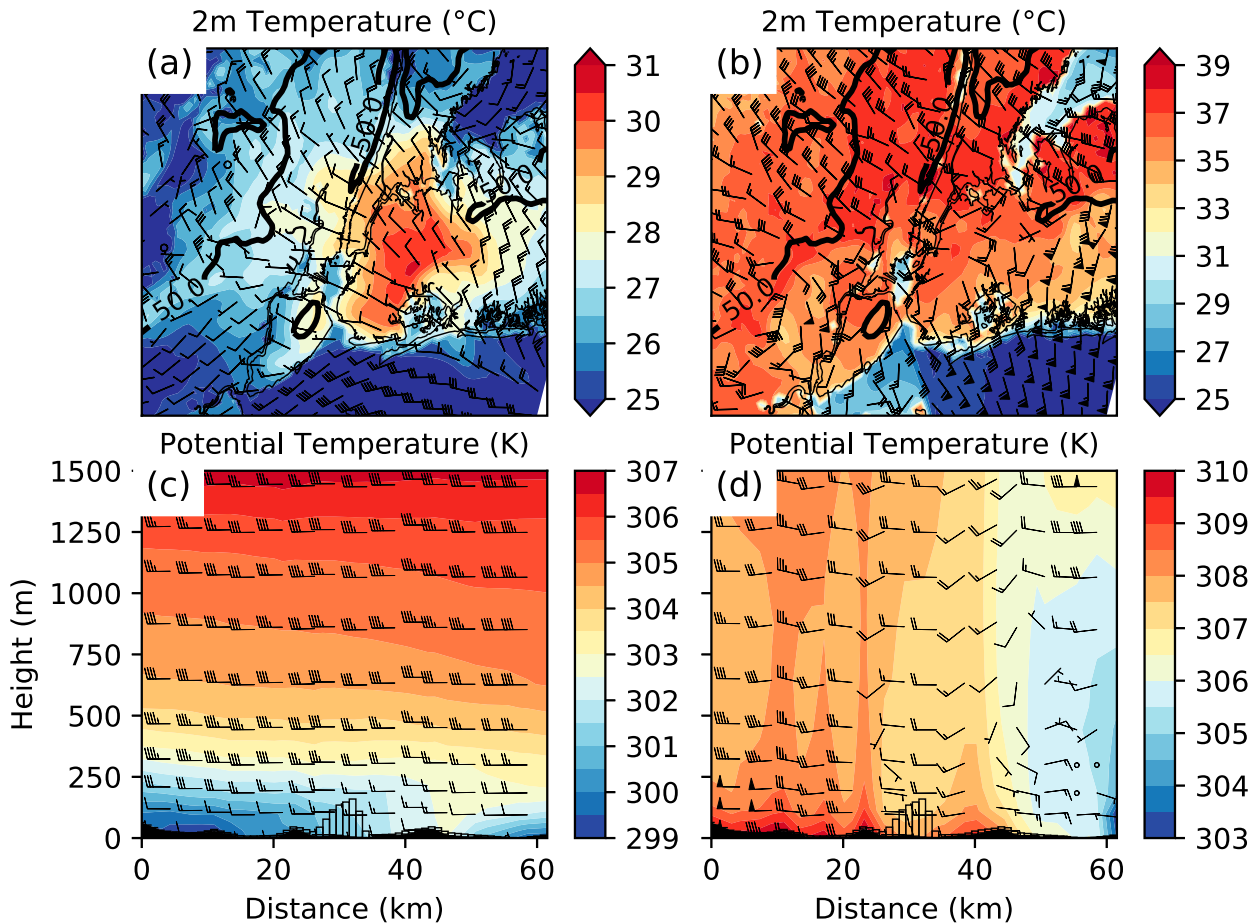


FIG. 6. Modeled 2-m air temperatures at (a) 0600 and (b) 1500 LST with all factors switched on. Also shown is the potential temperature vertical cross section along line AB at (c) 0600 and (d) 1500 LST. Unfilled bars represent gridpoint building heights. The wind-barb scale is as in Fig. 5. Black shading denotes the 50-m terrain height.

(2° – 3° C). This temperature gradient leads to a flow pattern that is similar to that observed in the urban surface factor (Fig. 7a), albeit with weaker magnitudes because of the weaker temperature contribution over the city.

Figure 8 shows contributions to temperature from all factors and their interactions at 0600 LST, close to the time of minimum temperature during the simulation period. Similar to afternoon temperature contributions, the urban land surface (Fig. 8a) increases temperatures. This positive temperature contribution is likely due to heat stored from incoming radiation throughout the day. The heat leads to warmer temperatures at the land surface because of the low thermal conductivity and high thermal storage of concrete (as well as other materials that are traditionally found in cities). The slab surface [parameterized in the Noah land surface model (LSM)] is therefore slow to cool, leading to increased upward sensible heat flux. Because sea surface temperatures are not affected by the urban surface, this positive contribution counteracts the westerly flow shown in Fig. 6.

The urban surface–urban fluxes interaction term (Fig. 8b) shows cooling of up to -1° C over the city, as in the afternoon. The frictional effects on the flow field oppose the baseline while adding to the synoptic flow. Although anthropogenic heat has been shown to increase urban temperatures, it interacts strongly (and negatively) with other factors such as impervious land surfaces, as shown in agreement with other studies (Ryu and Baik 2012). On a cool day (such as our no-heat-wave day), the 3D urban geometry stores less energy, thus contributing less to atmospheric temperatures. In addition, complex urban geometry provides a negative feedback to radiative cooling by having areas with sky-view factors of less than 1, partially blocking incoming radiation.

During the heat wave, the higher daytime temperatures at the urban surface lead to increased energy storage, in turn increasing nighttime sensible heat fluxes. This results in a positive contribution to nighttime temperatures of 2° – 3° C over Manhattan and

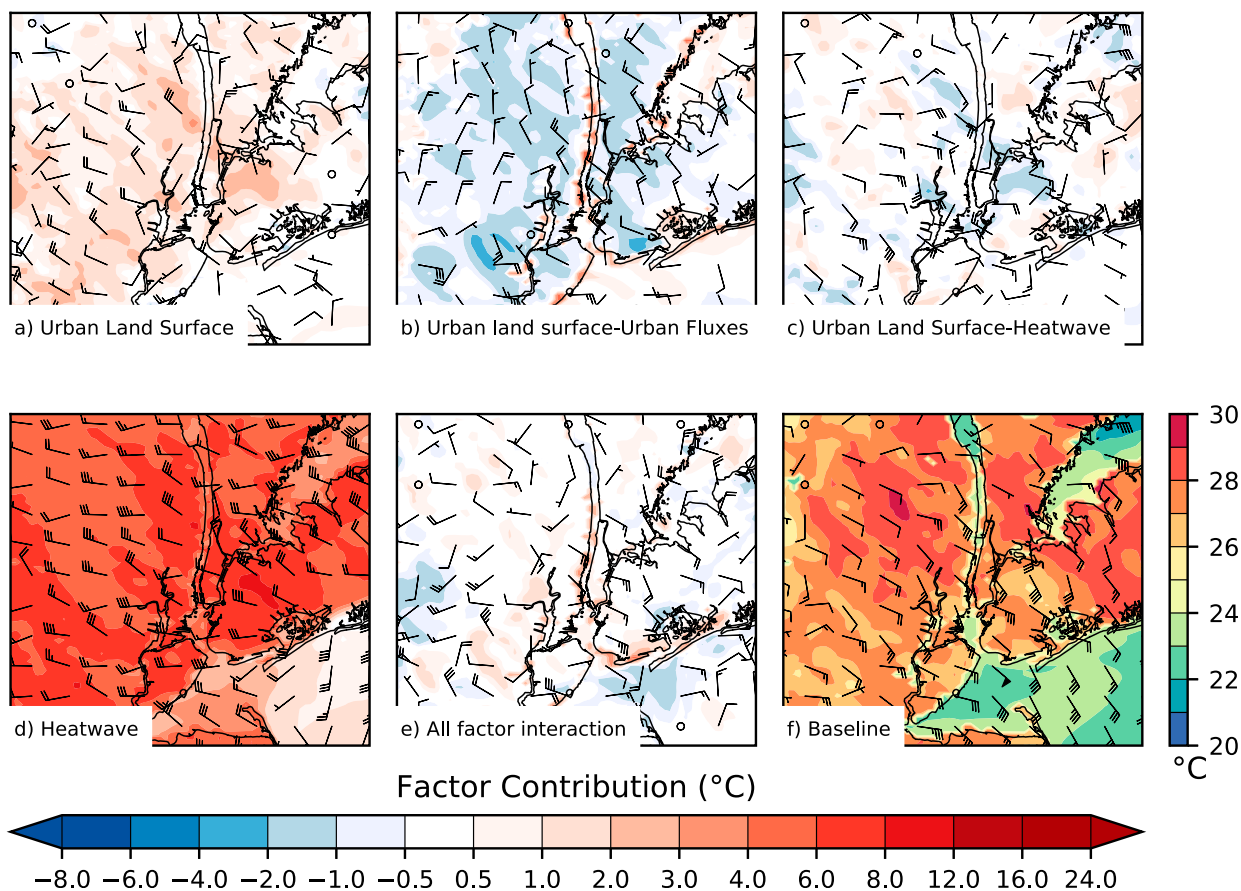


FIG. 7. Contribution of all factors and their interactions to modeled 2-m air temperature and 10-m winds at 1500 LST. The wind-barb scale is as in Fig. 5.

3°–4°C over Brooklyn and Queens (Fig. 8c). Once again, the flow-field contribution follows the positive temperature gradient, this time perturbing the total wind field from the northwesterly and westerly directions.

Synoptic conditions (Fig. 8d), as in afternoon hours, generate a westerly flow that is higher in magnitude than any other factor. As surface processes take on a more prominent role, synoptic conditions become less important, leading to near-0°C contributions. Synoptic conditions, however, have a nonlinear synergistic interaction with the urban surface, leading to an amplification of temperatures of 1°–3°C over the city (Fig. 8e). This all-factor interaction indicates an amplification of the UHI at night via positive feedbacks such as increased anthropogenic warming from air-conditioning use, slowing winds, and reduced evapotranspiration—conditions that have also been shown to be associated with the urban heat island. The wind pattern, as expected, opposes the prevalent winds as shown in Fig. 6a, contributing to the urban warming effect.

2) VERTICAL CROSS SECTION

This section explores impacts to potential temperature and wind vertical profiles within the NYC urban boundary layer through the cross section following line AB (Fig. 3), which passes from suburban New Jersey, through high rises in midtown Manhattan, all the way to Jamaica Bay.

In the afternoon, contributions from the urban surface represented by the slab parameterization in the Noah LSM (Fig. 9a) are positive and strongest closer to the ground. These positive impacts contribute to forming the superadiabatic layer seen in the total fields (Fig. 6d). This positive contribution extends to more than 600 m above the surface, consistent with findings from Bornstein (1968). Warming from the urban surface leads to convergence as seen in the horizontal fields, with contributions to wind speed of 0–2 m s⁻¹.

The urban surface and urban fluxes nonlinear interaction (Fig. 9b) has a positive impact on potential temperature over Manhattan while opposing the sea breeze. It nudges the atmosphere toward a negative

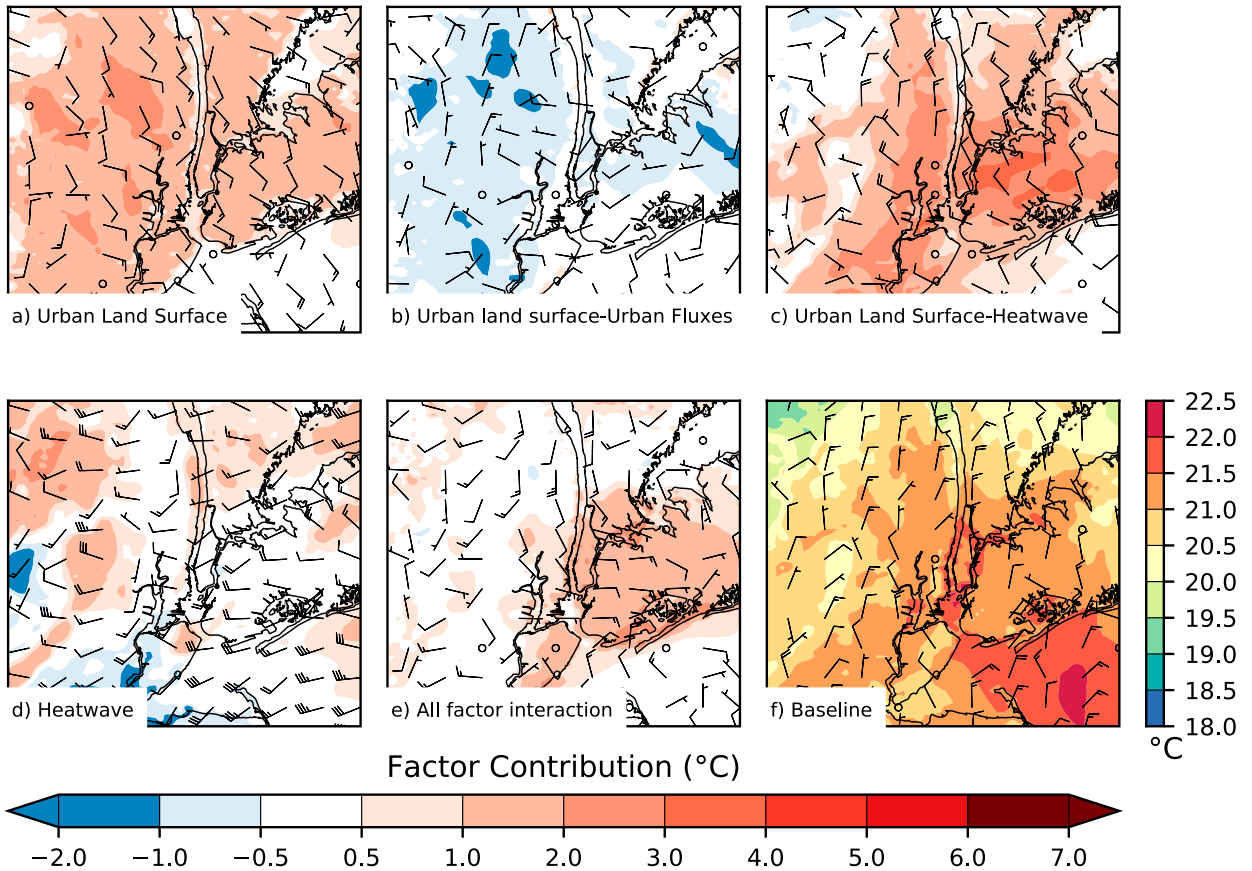


FIG. 8. As in Fig. 7, but at 0600 LST.

lapse rate, adding to the instability observed in the total fields (Fig. 6). Relative to the urban surface alone, the city, as represented by the modified BEP-BEM, releases a portion of the stored energy as latent heat from air conditioning while reducing sky-view factors from the ground.

A negative interaction is observed between the urban surface and heat wave (Fig. 9c). This contribution turns positive above 400 m, further perturbing the atmosphere toward the well-mixed conditions observed in Fig. 6d. This interaction factor opposes the synoptic flow, leading to cooling over the city

The heat-wave factor (Fig. 9d) dominates contributions to potential temperatures in the afternoon, reaching values up to 8 K near the surface. Wind contributions by this factor follow the anticyclonic flow generated by the high pressure system shown in Fig. 1. This contribution is largest outside Manhattan (distance > 30 km), over low-density residential grid points.

With the heat wave increasing energy loads on buildings, built surface temperatures increase, as does anthropogenic heating from air-conditioning use, yielding a positive contribution to the potential temperature field

(Fig. 9e) near the surface. This nonlinear interaction pushes the atmosphere toward unstable and well-mixed conditions. Closer to the coast, toward the end of the cross section, the interaction turns negative. The wind field opposes the synoptic flow near the start of the cross section because of the enhanced thermal gradient in urban surface temperatures.

At 0600 LST, UHI magnitude is at its highest over Brooklyn and Queens. The urban land surface (Fig. 10a), as represented by the Noah LSM slab parameterization, nudges the system toward a negative lapse rate, with enhanced warming below 400 m. Wind impacts are small (<1 m s⁻¹) and act against the direction observed in the total flow field (Fig. 6c) as the land-sea surface gradient is enhanced. When urban 3D geometry and urban fluxes are added (Fig. 10b), a portion of the building heat storage is rejected as latent heat, as formulated by Gutiérrez et al. (2015a). This represents a negative contribution in the context of the slab model in Fig. 10a, which rejects all energy stored by urban surfaces as sensible and radiative heating. This factor has an additive contribution to the total flow, albeit once again very weak and decreasing with height.

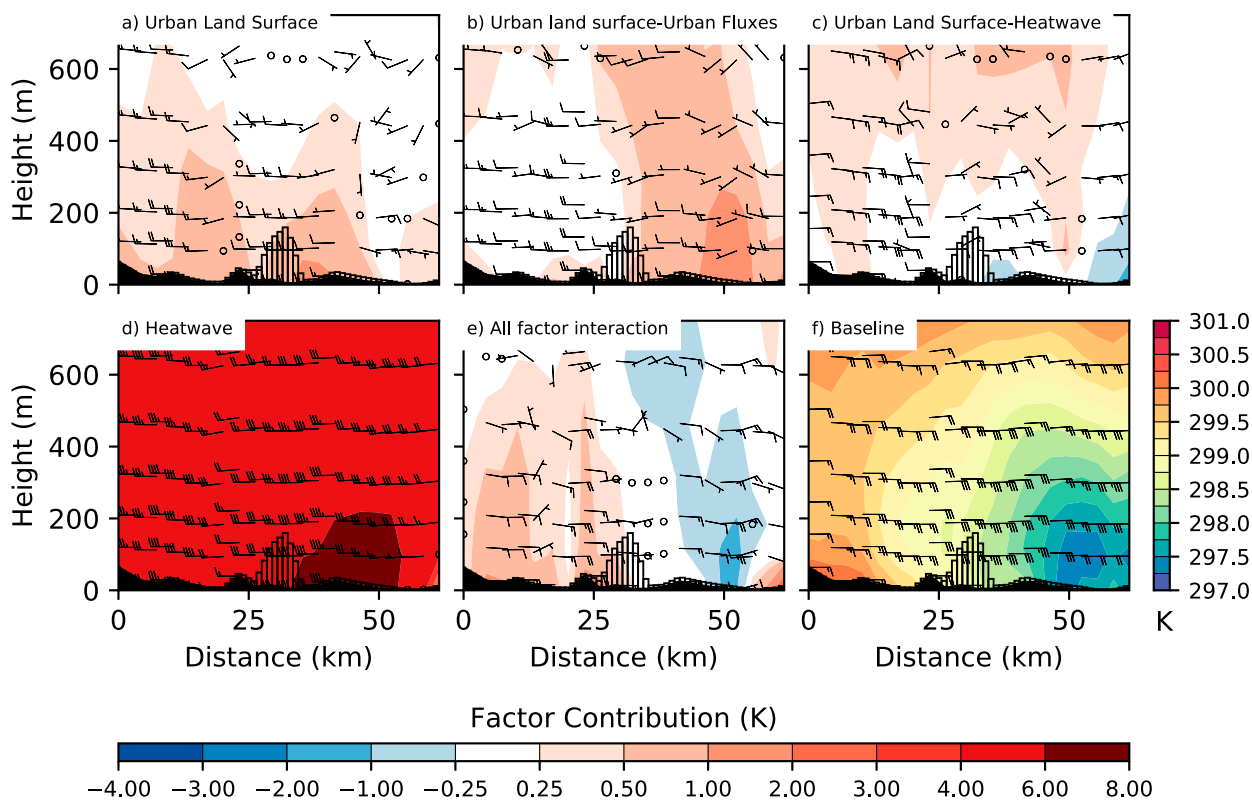


FIG. 9. Contribution of the three factors and their interactions to the potential temperature and wind vertical cross section through line AB at 1500 LST. The wind-barb scale is as in Fig. 5. Unfilled bars represent gridpoint building heights.

During heat-wave conditions, heat stored by the slab urban surface (Fig. 10c) increases, leading to increased losses through sensible heat flux and radiative cooling. This increase in temperature enhances the residual mixed layer observed over Brooklyn and Queens in the total flow and extends to around 300-m height, or around 1.5 times the mean building height over Manhattan. With surface effects taking more prominence at night, the heat-wave factor's relative impacts to potential temperature (Fig. 10d) decrease closer to ground level while providing the largest contribution to the westerly flow observed in Fig. 6c.

The impact observed in the interaction between urban surface and heat wave is further enhanced with the addition of anthropogenic heat and cooling from buildings. Likewise, less heat can be dissipated through radiative cooling because of interception by building walls. The thermal gradient acts in the direction of the heat wave's westerly flow.

Spatial distributions over the NYMA, both near the surface and in the cross sections that are shown here, hint at a change in surface-atmosphere interactions between nighttime and afternoon. At night, when the UHI is typically largest, urban surface factors are, in

aggregate, positive. Further, synoptic heat-wave conditions share many of the same aspects that are known to increase UHI, such as clear, dry nights with calm northwest winds, leading to synergistic interactions that amplify city temperatures. This nonlinear interaction can greatly increase UHI magnitude to over 5°C at night, as compared with 1.5°C (Fig. 11) outside the heat wave.

4. Summary and conclusions

The analysis presented in this article shows an application of the method of factor separation to assess contributions from 1) an urban surface, 2) a representation of the urban canopy (including anthropogenic, radiative, and dynamical effects), and 3) synoptic heat-wave conditions, as well as interactions between them over New York City for the 4–8 July 2010 heat wave. An updated urbanized WRF was used as the main simulation tool, improving the accuracy of surface temperatures relative to both reanalysis and the standard version of the model.

Analysis showed that both contributions from individual factors and their interactions are important. Nonlinear interactions between the surface and heat

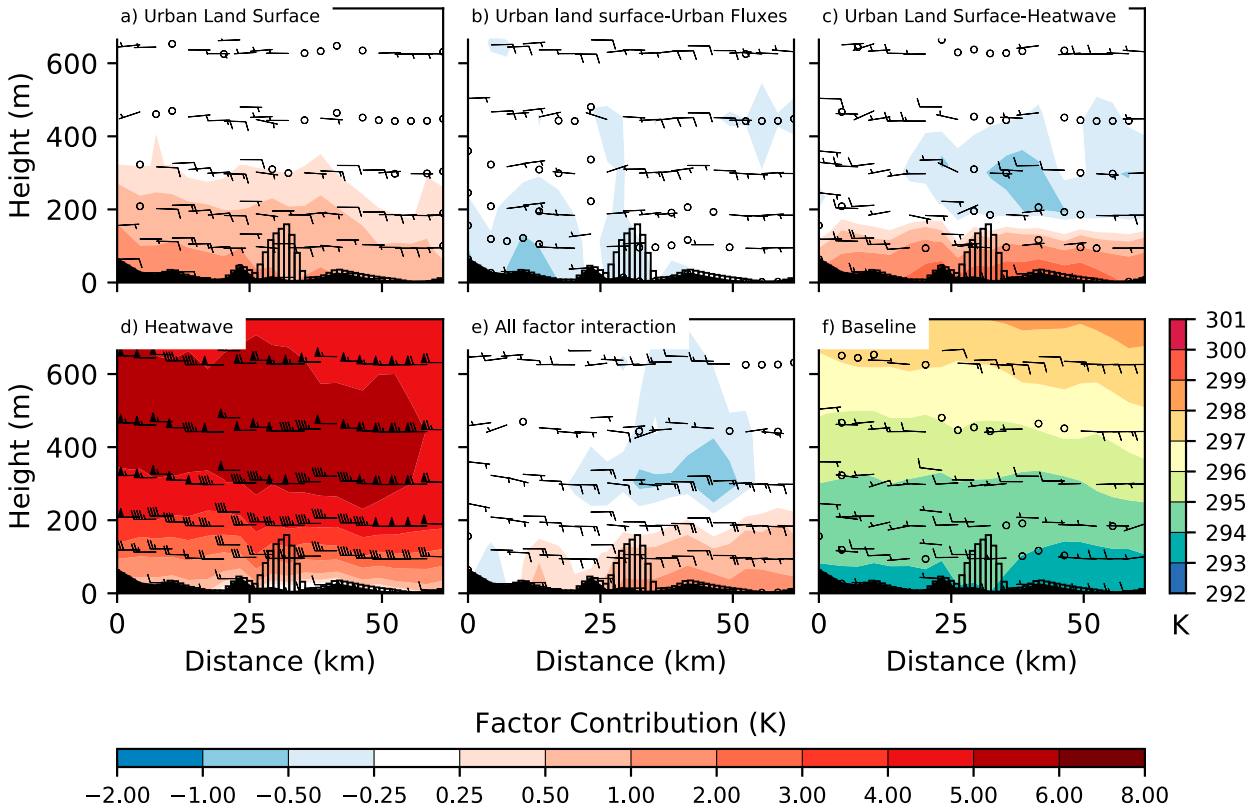


FIG. 10. As in Fig. 9, but at 0600 LST.

wave magnified the nighttime UHI by up to 6°C over parts of the city. Synoptic conditions dominated both 0600 and 1500 LST temperatures, with some factors matching its contributions over parts of Manhattan in the afternoon and over Brooklyn and Queens at night.

Results from the vertical structure show that the effects of the urban land cover and three-dimensional representation, as well as their interactions, follow patterns that are similar to those of the horizontal distributions. In general, contributions from urban land surface and urban parameterizations lessen with height, whereas the heat-wave contributions are larger above the surface. In the afternoon, the heterogeneous urban canopy modulates the vertical wind circulations. At 0600 LST, the wind pattern is dominated by the large-scale circulations and is enhanced by impervious land cover. Impervious land cover and the urban morphology contributions are larger during the afternoon, with the heat wave taking a more prominent role at night and in the early morning.

Although this work focuses on a single heat wave, its synoptic patterns are typical of heat waves in the northeastern United States, with a high pressure system stagnating over the Eastern Seaboard (or in some cases, just off the coast). Factor separation, as applied here, quantifies the UHI and its amplification during heat

waves. Results show that nonlinear interactions between the urban surface and synoptic heat-wave conditions can rival pure contributions from synoptic flows alone.

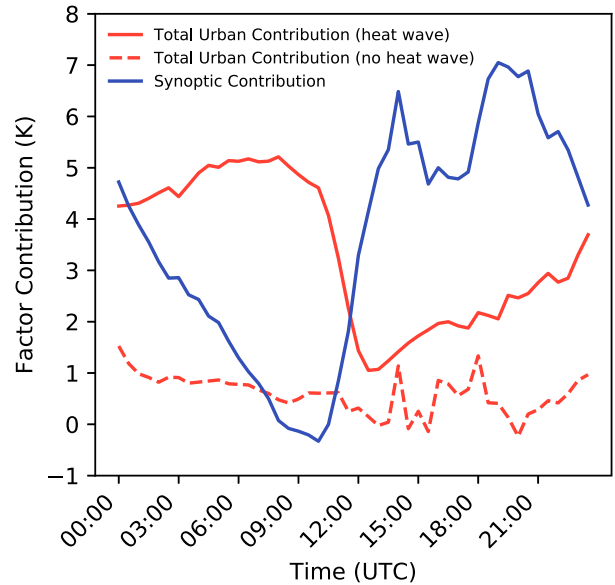


FIG. 11. Diurnal cycle of aggregated factor contributions to 2-m temperature from the city and synoptic heat-wave conditions.

This method can be applied to future climate-projection studies to account for biases due to urban fluxes under extreme-heat conditions. While heat-wave dynamics are not expected to change fundamentally from case to case, expanding the study to include more heat waves can strengthen results by reducing biases introduced by phenomena specific to this event (e.g., time of year, clouds, and initial soil conditions). Future work by the authors will focus on separating the aspects of the urban representation (i.e., anthropogenic heat vs building-geometry effects) to better understand how these factors interact under extreme-heat events, with application to projections of extreme-heat events throughout the twenty-first century. This study highlights how finescale surface-atmosphere interactions can rival even synoptic-level factors as a result of positive feedbacks. With urban populations growing worldwide, understanding how city temperatures change under heat waves improves our ability to assess their impacts.

Acknowledgments. The work presented here has been made possible through the NOAA-CREST Grant NA17AE1625. Computational resources were provided by the CUNY High Performance Computing Center, funded, in part, by grants from the City of New York, New York State, CUNY Research Foundation, and National Science Foundation Grants CNS-0958379, CNS-0855217, and ACI-1126113.

REFERENCES

- Anderson, G. B., and M. L. Bell, 2010: Heat waves in the United States: Mortality risk during heat waves and effect modification by heat wave characteristics in 43 U.S. communities. *Environ. Health Perspect.*, **119**, 210–218, <https://doi.org/10.1289/ehp.1002313>.
- Arend, M., D. Santoro, S. A. B. Gross, F. Moshary, and S. Ahmed, 2009: Development of a NYC meteorological network with emphasis on vertical wind profiles in support of meteorological and dispersion models. *Eighth Symp. on the Urban Environment*, Phoenix, AZ, Amer. Meteor. Soc., J1.2, <https://ams.confex.com/ams/pdfpapers/150289.pdf>.
- Basu, R., 2009: High ambient temperature and mortality: A review of epidemiologic studies from 2001 to 2008. *Environ. Health*, **8**, 40, <https://doi.org/10.1186/1476-069X-8-40>.
- Bornstein, R. D., 1968: Observations of the urban heat island effect in New York City. *J. Appl. Meteor.*, **7**, 575–582, [https://doi.org/10.1175/1520-0450\(1968\)007<0575:OOTUHI>2.0.CO;2](https://doi.org/10.1175/1520-0450(1968)007<0575:OOTUHI>2.0.CO;2).
- , and W. T. Thompson, 1981: Effects of frictionally retarded sea breeze and synoptic frontal passages on sulfur dioxide concentrations in New York City. *J. Appl. Meteor.*, **20**, 843–858, [https://doi.org/10.1175/1520-0450\(1981\)020<0843:EOFRSB>2.0.CO;2](https://doi.org/10.1175/1520-0450(1981)020<0843:EOFRSB>2.0.CO;2).
- Bougeault, P., and P. Lacarrere, 1989: Parameterization of orography-induced turbulence in a mesobeta-scale model. *Mon. Wea. Rev.*, **117**, 1872–1890, [https://doi.org/10.1175/1520-0493\(1989\)117<1872:POOITI>2.0.CO;2](https://doi.org/10.1175/1520-0493(1989)117<1872:POOITI>2.0.CO;2).
- Burian, S., N. Augustus, I. Jeyachandran, and M. Brown, 2008: National building statistics database. version 2. Los Alamos National Laboratory, http://www2.mmm.ucar.edu/wrf/src/wps_files/NUDAPT44_1km.tar.bz2.
- Charney, J. G., and J. G. DeVore, 1979: Multiple flow equilibria in the atmosphere and blocking. *J. Atmos. Sci.*, **36**, 1205–1216, [https://doi.org/10.1175/1520-0469\(1979\)036<1205:MFEITA>2.0.CO;2](https://doi.org/10.1175/1520-0469(1979)036<1205:MFEITA>2.0.CO;2).
- Comarazamy, D. E., J. E. González, J. C. Luvall, D. L. Rickman, and R. D. Bornstein, 2013: Climate impacts of land-cover and land-use changes in tropical islands under conditions of global climate change. *J. Climate*, **26**, 1535–1550, <https://doi.org/10.1175/JCLI-D-12-00087.1>.
- Curriero, F. C., K. S. Heiner, J. M. Samet, S. L. Zeger, L. Strug, and J. A. Patz, 2002: Temperature and mortality in 11 cities of the eastern United States. *Amer. J. Epidemiol.*, **155**, 80–87, <https://doi.org/10.1093/aje/155.1.80>.
- Dudhia, J., 1989: Numerical study of convection observed during the winter monsoon experiment using a mesoscale two-dimensional model. *J. Atmos. Sci.*, **46**, 3077–3107, [https://doi.org/10.1175/1520-0469\(1989\)046<3077:NSOCOD>2.0.CO;2](https://doi.org/10.1175/1520-0469(1989)046<3077:NSOCOD>2.0.CO;2).
- Gaffin, S. R., and Coauthors, 2008: Variations in New York City's urban heat island strength over time and space. *Theor. Appl. Climatol.*, **94**, 1–11, <https://doi.org/10.1007/s00704-007-0368-3>.
- Gedzelman, S. D., S. Austin, R. Cermak, N. Stefano, S. Partridge, S. Quesenberry, and D. A. Robinson, 2003: Mesoscale aspects of the urban heat island around New York City. *Theor. Appl. Climatol.*, **75**, 29–42, <https://doi.org/10.1007/s00704-002-0724-2>.
- Gutiérrez, E., 2016: Quantification of environmental impacts of heat fluxes from built environments. Ph.D. dissertation, The City College of New York, 310 pp., <https://search.proquest.com/openview/ec0a7802671404720bef2da0c9bdc585/1?pq-origsite=gscholar&cbl=18750&diss=y>.
- , J. E. González, A. Martilli, and R. Bornstein, 2015a: On the anthropogenic heat fluxes using an air conditioning evaporative cooling parameterization for mesoscale urban canopy models. *J. Sol. Energy Eng.*, **137**, 051005, <https://doi.org/10.1115/1.4030854>.
- , —, —, —, and M. Arend, 2015b: Simulations of a heat-wave event in New York City using a multilayer urban parameterization. *J. Appl. Meteor. Climatol.*, **54**, 283–301, <https://doi.org/10.1175/JAMC-D-14-0028.1>.
- , A. Martilli, J. L. Santiago, and J. E. González, 2015c: A mechanical drag coefficient formulation and urban canopy parameter assimilation technique for complex urban environments. *Bound.-Layer Meteor.*, **157**, 333–341, <https://doi.org/10.1007/s10546-015-0051-7>.
- Hong, S.-Y., and J.-O. J. Lim, 2006: The WRF single-moment 6-class microphysics scheme (WSM6). *Asia-Pac. J. Atmos. Sci.*, **42**, 129–151.
- Kain, J. S., 2004: The Kain-Fritsch convective parameterization: An update. *J. Appl. Meteor.*, **43**, 170–181, [https://doi.org/10.1175/1520-0450\(2004\)043<0170:TKCPAU>2.0.CO;2](https://doi.org/10.1175/1520-0450(2004)043<0170:TKCPAU>2.0.CO;2).
- Le Comte, D. M., and H. E. Warren, 1981: Modeling the impact of summer temperatures on national electricity consumption. *J. Appl. Meteor.*, **20**, 1415–1419, [https://doi.org/10.1175/1520-0450\(1981\)020<1415:MTIOST>2.0.CO;2](https://doi.org/10.1175/1520-0450(1981)020<1415:MTIOST>2.0.CO;2).
- Li, D., and E. Bou-Zeid, 2013: Synergistic interactions between urban heat islands and heat waves: The impact in cities is larger than the sum of its parts. *J. Appl. Meteor. Climatol.*, **52**, 2051–2064, <https://doi.org/10.1175/JAMC-D-13-02.1>.
- Madrigano, J., D. Jack, G. Anderson, M. Bell, and P. Kinney, 2015: Temperature, ozone, and mortality in urban and non-urban

- counties in the northeastern United States. *Environ. Health*, **14**, 3, <https://doi.org/10.1186/1476-069X-14-3>.
- Martilli, A., 2002: Numerical study of urban impact on boundary layer structure: Sensitivity to wind speed, urban morphology, and rural soil moisture. *J. Appl. Meteor.*, **41**, 1247–1266, [https://doi.org/10.1175/1520-0450\(2002\)041<1247:NSOUJO>2.0.CO;2](https://doi.org/10.1175/1520-0450(2002)041<1247:NSOUJO>2.0.CO;2).
- , A. Clappier, and M. W. Rotach, 2002: An urban surface exchange parameterisation for mesoscale models. *Bound.-Layer Meteor.*, **104**, 261–304, <https://doi.org/10.1023/A:1016099921195>.
- McGeehin, M. A., and M. Mirabelli, 2001: The potential impacts of climate variability and change on temperature-related morbidity and mortality in the United States. *Environ. Health Perspect.*, **109**, 185–189, <https://doi.org/10.2307/3435008>.
- Meehl, G. A., and C. Tebaldi, 2004: More intense, more frequent, and longer lasting heat waves in the 21st century. *Science*, **305**, 994–997, <https://doi.org/10.1126/science.1098704>.
- Meir, T., P. M. Orton, J. Pullen, T. Holt, W. T. Thompson, and M. F. Arend, 2013: Forecasting the New York City urban heat island and sea breeze during extreme heat events. *Wea. Forecasting*, **28**, 1460–1477, <https://doi.org/10.1175/WAF-D-13-00012.1>.
- Mesinger, F., and Coauthors, 2006: North American Regional Reanalysis. *Bull. Amer. Meteor. Soc.*, **87**, 343–360, <https://doi.org/10.1175/BAMS-87-3-343>.
- Miller, N. L., K. Hayhoe, J. Jin, and M. Auffhammer, 2008: Climate, extreme heat, and electricity demand in California. *J. Appl. Meteor. Climatol.*, **47**, 1834–1844, <https://doi.org/10.1175/2007JAMC1480.1>.
- Mlawer, E. J., S. J. Taubman, P. D. Brown, M. J. Iacono, and S. A. Clough, 1997: Radiative transfer for inhomogeneous atmospheres: RRTM, a validated correlated-*k* model for the longwave. *J. Geophys. Res.*, **102**, 16 663–16 682, <https://doi.org/10.1029/97JD00237>.
- National Weather Service, 2015: Natural hazard statistics. Accessed 20 November 2015, <http://www.nws.noaa.gov/om/hazstats.shtml>.
- Niyogi, D., T. Holt, S. Zhong, P. C. Pyle, and J. Basara, 2006: Urban and land surface effects on the 30 July 2003 mesoscale convective system event observed in the southern Great Plains. *J. Geophys. Res.*, **111**, D19107, <https://doi.org/10.1029/2005JD006746>.
- Oke, T. R., 1988: Street design and urban canopy layer climate. *Energy Build.*, **11**, 103–113, [https://doi.org/10.1016/0378-7788\(88\)90026-6](https://doi.org/10.1016/0378-7788(88)90026-6).
- Robinson, P. J., 2001: On the definition of a heat wave. *J. Appl. Meteor.*, **40**, 762–775, [https://doi.org/10.1175/1520-0450\(2001\)040<0762:OTDOAH>2.0.CO;2](https://doi.org/10.1175/1520-0450(2001)040<0762:OTDOAH>2.0.CO;2).
- Ronda, R. J., G. J. Steeneveld, B. G. Heusinkveld, J. J. Attema, and A. A. M. Holtslag, 2017: Urban finescale forecasting reveals weather conditions with unprecedented detail. *Bull. Amer. Meteor. Soc.*, **98**, 2675–2688, <https://doi.org/10.1175/BAMS-D-16-0297.1>.
- Ryu, Y.-H., and J.-J. Baik, 2012: Quantitative analysis of factors contributing to urban heat island intensity. *J. Appl. Meteor. Climatol.*, **51**, 842–854, <https://doi.org/10.1175/JAMC-D-11-098.1>.
- Salamanca, F., A. Krpo, A. Martilli, and A. Clappier, 2010: A new building energy model coupled with an urban canopy parameterization for urban climate simulations—Part I. Formulation, verification, and sensitivity analysis of the model. *Theor. Appl. Climatol.*, **99**, 331–344, <https://doi.org/10.1007/s00704-009-0142-9>.
- Santamouris, M., N. Papanikolaou, I. Livada, I. Koronakis, C. Georgakis, A. Argiriou, and D. Assimakopoulos, 2001: On the impact of urban climate on the energy consumption of buildings. *Sol. Energy*, **70**, 201–216, [https://doi.org/10.1016/S0038-092X\(00\)00095-5](https://doi.org/10.1016/S0038-092X(00)00095-5).
- Sequera, P., J. E. González, K. McDonald, R. Bornstein, and D. Comarazamy, 2015: Combined impacts of land cover changes and large-scale forcing on southern California summer daily maximum temperatures. *J. Geophys. Res. Atmos.*, **120**, 9208–9219, <https://doi.org/10.1002/2015JD023536>.
- Skamarock, W. C., and Coauthors, 2008: A description of the Advanced Research WRF version 3. NCAR Tech. Note NCAR/TN-475+STR, 113 pp., <http://dx.doi.org/10.5065/D68S4MVH>.
- Stein, U., and P. Alpert, 1993: Factor separation in numerical simulations. *J. Atmos. Sci.*, **50**, 2107–2115, [https://doi.org/10.1175/1520-0469\(1993\)050<2107:FSINS>2.0.CO;2](https://doi.org/10.1175/1520-0469(1993)050<2107:FSINS>2.0.CO;2).
- Tewari, M., and Coauthors, 2004: Implementation and verification of the unified Noah land surface model in the WRF Model. *20th Conf. on Weather Analysis and Forecasting/16th Conf. on Numerical Weather Prediction*, Seattle, WA, Amer. Meteor. Soc., 14.2a, <https://ams.confex.com/ams/pdfpapers/69061.pdf>.